

Title:

FDTD and Elastic Continuum Analysis of the Liquid Crystal Polarization Grating

Authors:

Chulwoo Oh, Ravi Komanduri, and Michael J. Escuti

Affiliation:

North Carolina State University, Dept Electrical & Computer Engineering, Raleigh, NC (USA)

Presented At:

SID International Symposium, Seminar, and Exhibition, San Francisco, CA (June 4-9, 2006)

Citation:

C. Oh, R. Komanduri, and M. J. Escuti, " FDTD and Elastic Continuum Analysis of the Liquid Crystal Polarization Grating," *SID Symposium Digest*, **vol. 37**, pp. 844-847, (2006).

Copyright 2006 Society For Information Display.

This paper was published in the SID Symposium Digest Vol. 37 and is made available as an electronic reprint. One print or electronic copy may be made for personal use only. Systematic or multiple reproduction, distribution to multiple locations via electronic or other means, duplication of any material in this paper for a fee or for commercial purposes, or modification of the content of this paper are prohibited.

P-167: FDTD and Elastic Continuum Analysis of the Liquid Crystal Polarization Grating

Chulwoo Oh, Ravi Komanduri, and Michael J. Escuti¹

Dept of Electrical and Computer Engineering, North Carolina State University, Raleigh, NC, USA

Abstract

The liquid crystal polarization grating (LCPG) has advantages of polarization independence of the zero diffraction order, nearly 100% diffraction efficiency in the first orders, and higher resolution capability over previously reported binary LC gratings. Here we analyze the LCPG, an electrically controlled, polarization-independent light modulator using the finite-difference time-domain (FDTD) method and the elastic continuum theory. The optical performance is studied and critical electrical parameters for a LCPG cell are presented.

1. Introduction

A number of liquid crystal (LC) light modulators operating on unpolarized light have been proposed in an effort to overcome the substantial losses in conventional LC displays that require polarized light. Most prominently, Bos and coworkers suggested several potentially efficient and polarization-independent diffraction gratings using liquid crystals [1-4]. These approaches, however, face crucial limitations for real applications due to their binary nature: fabrication difficulty and the easy appearance of defects. They therefore tend to have inherently large periods that result in many diffraction orders with small diffraction angles.

A newly demonstrated liquid crystal polarization grating (LCPG) [5] is a switchable diffractive optical element with a continuously varying, periodic, anisotropic index profile. As shown in Fig. 1(a), this can be embodied as a nematic director that follows [6]:

$$\mathbf{n}(x) = \hat{\mathbf{x}} \cos(\pi x / \Lambda) + \hat{\mathbf{y}} \sin(\pi x / \Lambda) + \hat{\mathbf{z}}(0) \quad (1)$$

where Λ is half of the period of the nematic director. It has been shown [5] in experiment and in theory that the diffraction from this LCPG can be summarized by:

$$\eta_0 = \cos^2\left(\frac{\pi \Delta n d}{\lambda}\right) \quad \text{and} \quad \eta_{\pm 1} = \frac{1 \mp S'_3}{2} \sin^2\left(\frac{\pi \Delta n d}{\lambda}\right) \quad (2)$$

where η_m is the diffraction efficiency of the m^{th} -order, Δn is the LC birefringence, d is the cell gap, λ is the free-space wavelength, and $S'_3 = S_3/S_0$ is the normalized Stokes parameter corresponding to ellipticity of the incident light [7]. The compelling experimentally confirmed advantage [5,8] of this LCPG over other LC modulators is that *unpolarized light can be modulated with high contrast* at low-to-moderate drive voltages.

While analytic expressions derived for the diffraction of this PG are useful, they have not yet been confirmed with numerical simulation. It is also not clear how many grating periods within a single pixel are required to get high diffraction efficiency. Furthermore, we seek to better understand the static and dynamic thresholds required for good alignment of the nematic director.

First, we examine the optical performance of LCPGs in comparison to Eq. (2) and to previously reported LC gratings. To

do this, we implemented a 2D Finite-Difference Time-Domain (FDTD) method [9-11] for periodic anisotropic structures.

Second, we examine the alignment and voltage response properties of the LCPG using Elastic Continuum theory [12], deriving analytic expressions for the critical thickness, voltage threshold, and switching times. We go beyond the one constant approximation [13] previously used, and present the analytic expressions for the more general two-constant case ($K_3=K_1 \neq K_2$).

2. Finite-Difference Time-Domain Simulations

The FDTD method derives its name from the direct solution of Maxwell's curl equations:

$$j\omega\epsilon_0\tilde{\epsilon}\mathbf{E} = \nabla \times \mathbf{H} \quad \text{and} \quad j\omega\mu_0\mathbf{H} = -\nabla \times \mathbf{E} \quad (3)$$

For the well-aligned LCPG with the texture dictated by Eq. (1), the optical dielectric tensor $\tilde{\epsilon}$ corresponding to the LC director profile is periodic along \hat{x} and varies with respect to (x, y) :

$$\tilde{\epsilon} = \begin{bmatrix} \epsilon_{\perp} \sin^2 \phi + \epsilon_e \cos^2 \phi & \Delta \epsilon \sin \phi \cos \phi & 0 \\ \Delta \epsilon \sin \phi \cos \phi & \epsilon_{\perp} \cos^2 \phi + \epsilon_{//} \sin^2 \phi & 0 \\ 0 & 0 & \epsilon_{\perp} \end{bmatrix} \quad (4)$$

where ϵ_{\perp} and $\epsilon_{//}$ are the ordinary (perpendicular) and extraordinary

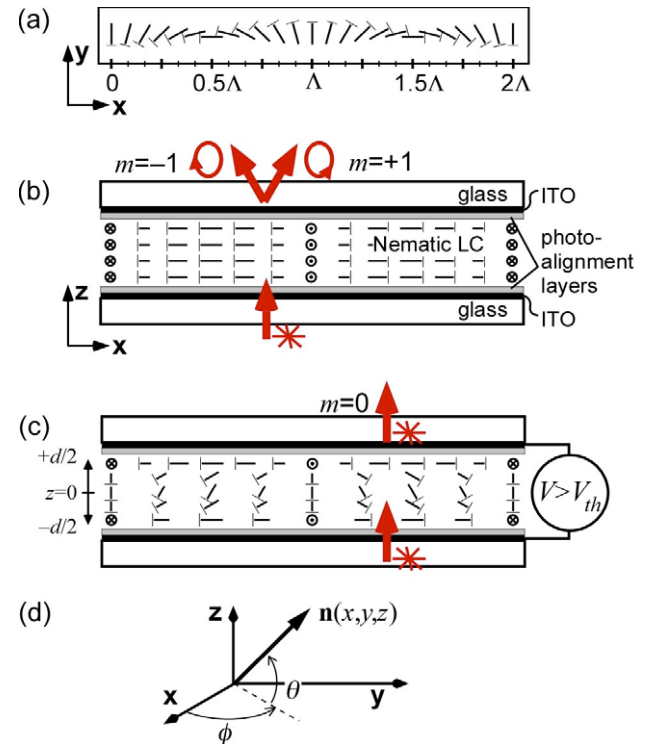


Fig 1: LCPG director: (a) top-view, (b) side-view of the well-aligned diffracting state ($V < V_{th}$ and $d < d_c$), (c) side-view when thresholds are exceeded ($V > V_{th}$ or $d > d_c$), and (d) geometry.

¹ Preferred email contact: mjescuti@ncsu.edu

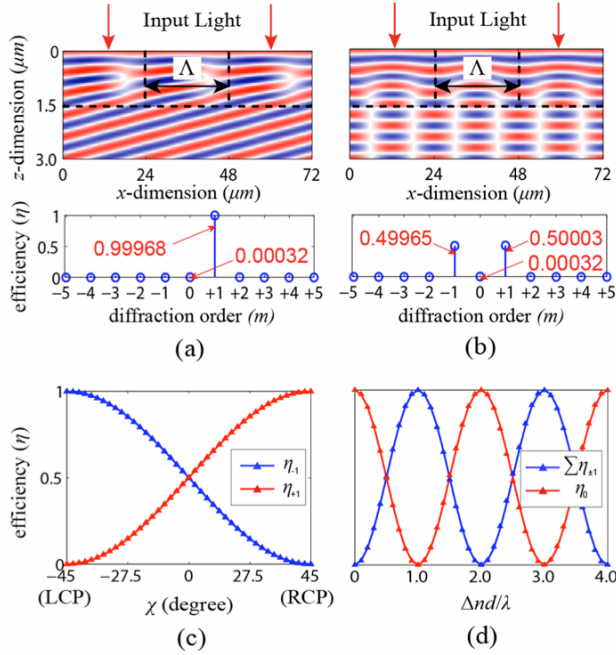


Fig 2: Calculated FDTD near-field (E_y) map and far-field diffraction of the LCPG for (a) circular and (b) linear input polarization. Calculated far-field diffraction efficiency (solid-lines for theory; triangles for FDTD) as a function of (c) the ellipticity of the input polarization χ , and (d) the normalized parameter $\Delta nd/\lambda$. (note: $\Lambda=40\lambda$, $d=\lambda/2\Delta n$, and $\Delta n=0.2$).

(parallel) relative dielectric constants, $\Delta\epsilon = (\epsilon_{//} - \epsilon_{\perp})$ is the dielectric anisotropy, and $\phi = \pi x/\Lambda$. While it is desirable to reduce the computation space to a unit cell by applying periodic boundary conditions, this involves considerable complexity to handle waves propagating at oblique directions. This difficulty can be circumvented using a new set of field variables [10]: $\mathbf{P} = \mathbf{E} \exp(jk_x x)$ and $\mathbf{Q} = 120\pi \mathbf{H} \exp(jk_x x)$. Eq. (3) now becomes:

$$\frac{j\omega}{c} \mathbf{P} = \tilde{\epsilon}^{-1} (\nabla \times \mathbf{Q}) \quad \text{and} \quad \frac{j\omega}{c} \mathbf{Q} = -\nabla \times \mathbf{P}. \quad (5)$$

We solve these modified Maxwell's equations by the split-field update method [10]. The two boundaries along \hat{z} must be appropriately terminated to avoid non-physical reflections, so we construct absorbing boundaries using the Uniaxial Perfectly Matched Layers (UPML) technique [11]. For our simulations, the maximum grid spacing was $1/40^{\text{th}}$ of the center wavelength and the Courant stability factor was $1/3$. We used a Gaussian pulse for evaluating the spectral characteristics.

2.1 FDTD Diffraction Characteristics

The most unique feature of the LCPG is its 100% diffraction (a Bragg property), even though it falls into the Raman-Nath grating regime. Fig 2(a) and (b) shows the near-field images and diffraction efficiencies of the FDTD simulation for circular and linear input polarization when $\Delta nd/\lambda=0.5$. We generally find all aspects of Eq. (1) reflected in the FDTD simulations, especially the polarization independence of the 0th-order. The $\pm 1^{\text{st}}$ -order diffraction for various input polarizations is shown in Fig. 2(c) (and $\eta_{+1}=\eta_{-1}$ for all linear polarization). The spectral response of the LCPG is presented in Fig. 2(d).

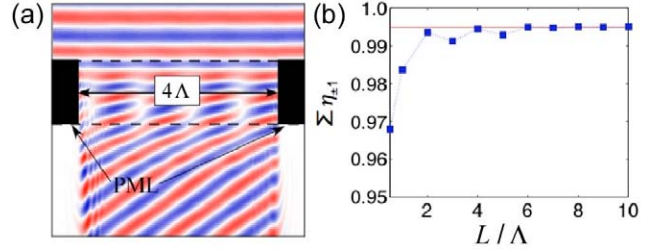


Fig 3: LCPG within a single small pixel: (a) near-field map of the electric field and (b) far-field diffraction efficiency of the sum of the first orders for various pixel sizes L/Λ with $\Lambda=10\lambda$.

2.2 Minimum LCPG Pixel Size Study

We also seek to estimate the minimum pixel size that can be used with the LCPG modulator. To answer this, we model a pixel aperture (width L) with PML layers (Fig. 3(a)) and compare the far-field intensities with and without the LCPG structure. Our intent is to isolate identify the maximum diffraction efficiency of a single pixel, and the minimum pixel size may be determined by as the smallest L that supports strong diffraction. Fig. 3 shows the field map of the FDTD simulation and the diffraction efficiency (a sum of $\eta_{\pm 1}$) vs. pixel size. The diffraction efficiency asymptotically approaches a nearly ideal value (99.5%) when $L/\Lambda \geq 4$. Since we expect that future experimental minimum periods are $\sim 5 \mu\text{m}$ [5], it appears likely that the minimum pixel size will be $\sim 20\mu\text{m}$. In applications where a slight decrease in efficiency is tolerable, the pixel size could be as small as $L/\Lambda = 2$.

2.3 Comparison of LCPG with other gratings

The most comparable previous LC gratings, the Reverse Twist Grating (RTG) [1] and Hybrid LC Grating (HG) [2], are illustrated in Fig. 4(a) and (b). Adjacent LC domains of the RTG have the opposite twist sense (a high pre-tilt angle is safely ignored for the optical simulation). The HG employs hybrid surface orientations – planar and homeotropic texture, with adjacent cells having orthogonal alignment. We assume that the tilt angle for the HG cell varies linearly along the thickness of the cell [2]. Note that the discrete nature of the LC configuration in all binary LC gratings leads to strong disclinations within each grating period that reduce the maximum efficiency [3] and contrast ratio.

The FDTD predictions of diffraction efficiencies reveal that all three gratings under consideration could yield 100%-diffraction

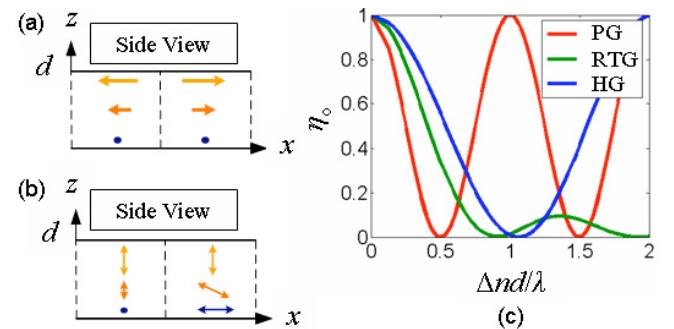


Fig 4: Comparisons of the LCPG with RTG and HP gratings: illustrations of one period of the (a) RTG and (b) HG gratings; and (c) the simulated 0th-order efficiencies.

efficiency and polarization-independence (in principle). The ideal efficiencies in the 0th-order are presented as a function of $\Delta nd/\lambda$ in Fig. 3(c). For the RTG, the maximum diffraction occurs when $\Delta nd/\lambda$ values satisfy the Gooch and Tarry minima conditions. The HG and LCPG structures produce maximum diffraction when grating parameters satisfy the conditions for $\lambda/2$ retardation since both diffract based on retardation. Note that the HG thickness for $\lambda/2$ retardation is doubled since the average birefringence of the HG cell is $\Delta n/2$. However, the LCPG has only three orders of diffraction (the 0th- and $\pm 1^{\text{st}}$ -orders), while the other gratings always have a large number of diffraction orders.

3. Elastic continuum analysis of LCPG

In order to achieve the compelling optical features predicted by the FDTD analysis above, it is essential that the LC nematic director configuration follow Eq. (1). As shown in an earlier work [13], this in-plane texture will only be possible when the thickness of the LC layer (d) is below a critical thickness (d_c) or when the applied voltage (V) is less than a voltage threshold (V_{th}). After fabricating well-aligned LCPG samples, we noticed that the previously reported expression for critical thickness was far too optimistic (too large), primarily because it assumed by a one-constant approximation. Furthermore, there has not been any theoretical analysis of the switching times. Here we aim to determine more general analytic expressions for these parameters.

For nematic LCs, the uniaxial nature of the molecules can be described by means of the nematic director (\mathbf{n}). It can be completely described by two angles (Fig. 1(d)):

$$\mathbf{n}(x, z) = \hat{\mathbf{x}} \cos \theta \cos \phi + \hat{\mathbf{y}} \cos \theta \sin \phi + \hat{\mathbf{z}} \sin \theta \quad (6)$$

Here $\theta(x, z)$ and $\phi(x, z)$ are the tilt and azimuth angles of the nematic director, respectively. Here, we assume the following:

- i. At the substrate surfaces strong anchoring conditions exist which ensure that $\theta = 0$ and $\phi = \pi x/\Lambda$ always at $z = \pm d/2$.
- ii. θ and ϕ are independent of each other. More specifically, $\theta(z)$ and $\phi(x)$ (illustrated in Fig. 1). While this may not ultimately be true for all electric field values, we anticipate it is valid for low fields.
- iii. When $V > V_{th}$, we assume that the tilt angle profile is symmetric about the center of the sample, $\theta(z) = \theta(-z)$ [12].
- iv. The maximum tilt angle (θ_{max}) at any equilibrium state occurs at the center of the sample, $\theta(z=0) = \theta_{max}$ and $\partial \theta / \partial z|_{z=0} = 0$.
- v. The bend and splay elastic constants are identical ($K = K_3 = K_1$) while the twist elastic constant (K_2) is distinct. This two-constant approximation is a slightly general formulation of the more common one-constant approximation (OCA).

The Frank-Oseen elastic energy density [12] including the splay, twist, and bend deformations,

$$\omega_F = \frac{1}{2} K_1 (\nabla \cdot \mathbf{n})^2 + \frac{1}{2} K_2 (\mathbf{n} \cdot \nabla \times \mathbf{n})^2 + \frac{1}{2} K_3 (\mathbf{n} \times \nabla \times \mathbf{n})^2, \quad (7)$$

can be simplified with the above assumptions and Eq. (6) to

$$\omega_F = f(\theta, \phi) \left(\frac{d\phi}{dx} \right)^2 + g(\theta, \phi) \left(\frac{d\theta}{dz} \right)^2 + h(\theta, \phi) \left(\frac{d\phi}{dx} \right) \left(\frac{d\theta}{dz} \right) \quad (8)$$

where

$$f(\theta, \phi) = \frac{\cos^2 \theta}{2} \left[\begin{array}{l} (K - K_2 \sin^2 \theta - K \cos^2 \theta) \sin^2 \phi \\ + K_2 \sin^2 \theta + K \cos^2 \theta \end{array} \right] \quad (9a)$$

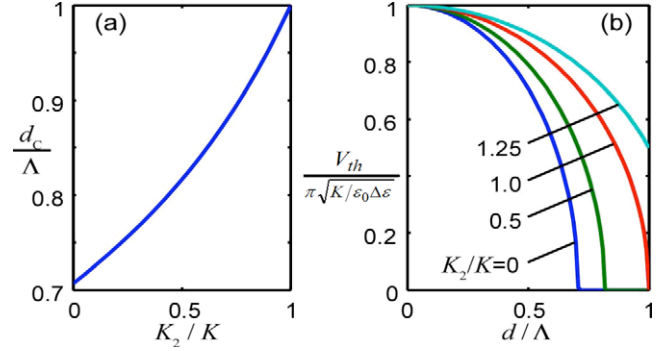


Fig 5: Theoretical (a) critical thickness and (b) voltage threshold assuming a two-constant approximation ($K_1=K_3$).

$$g(\theta) = K/2. \quad (9b)$$

We do not explicitly show $h(\theta, \phi)$ since it does not appear in the equilibrium equations. Since we seek solutions around the threshold (i.e. $\theta \approx 0$), $\cos \theta \approx 1$ and $\sin \theta \approx 0$. Under this condition, the coefficient of $\sin^2 \phi$ in equation (9a) is small and is neglected. Therefore, we assume $f(\theta) \sim \cos^2(\theta/2) [K_2 \sin^2 \theta + K \cos^2 \theta]$ near the threshold conditions. By minimizing the energy density using variational principles [12], we get the equilibrium equations:

$$2f(\theta) \frac{d}{dx} \left(\frac{d\phi}{dx} \right) = 0 \quad (10)$$

$$2g(\theta) \frac{d}{dz} \left(\frac{d\theta}{dz} \right) - \frac{\partial}{\partial \theta} (f(\theta)) \left(\frac{d\phi}{dx} \right)^2 = 0. \quad (11)$$

The first equation leads to a linear solution for the azimuth angle ϕ , which matches with our boundary conditions. Using the above static equations, we can identify critical thicknesses. By adding the electric field energy to Eq. (7) and using the same assumptions as before, we can estimate the voltage threshold. For evaluating the response times we have to resort to the dynamic equations. In each of these cases, we are solving for the polar angle θ .

3.1 Critical thickness

Using Eq. (11) and substituting $\Omega = \sin^{-1}(\sin(\theta)/\sin(\theta_{max}))$, the following relation between d and θ_{max} can be obtained.

$$\int_0^{\pi/2} \frac{\cos \Omega \partial \Omega}{\sqrt{2(1 - \sin^2 \Omega \sin^2 \theta_{max})(f(\theta) - f(\theta_{max}))(K \sin \theta_{max})^{-1}}} = \frac{\pi d}{\Lambda^2} \quad (12)$$

Using the simplified expression for $f(\theta)$, we simplify the integrand in Eq. (12) and then substitute $\theta_{max} = 0$ to get the following value for the critical thickness.

$$d_c = \Lambda (2 - K_2/K)^{-1/2} \quad (13)$$

Substituting $K_2=K$ in the above expression gives $d_c = \Lambda$, which matches with the previous result [13], that was derived using dynamic arguments. The normalized critical thickness is shown in Fig. 5(a), highlighting its tendency to monotonically increase as the elastic constants become more similar. This helps to explain why in our experiments we find that the critical thickness is dramatically lower than $d_c = \Lambda$. This result is additionally important since it predicts that the smallest grating periods are formed with nematic LCs with larger K_2/K ratios.

3.2 Voltage Threshold

To analyze the influence of applied voltage on the LC orientation, the electric energy term has to be added to the elastic energy expression in Eq. (7). Then the minimization condition on the total energy yields a relation that which can be solved [12] for V_{th} once again by substituting $\theta_{max} = 0$. The resultant expression for threshold voltage is given by

$$V_{th} = \pi \sqrt{\frac{K}{\epsilon_0 \Delta \epsilon} \left(1 - \left(\frac{d}{d_c} \right)^2 \right)} \quad (14)$$

In the above expression d_c is the critical thickness given by Eq. (13), and it is assumed $d < d_c$. By considering the OCA case, we find the result previously derived [13-14]. The expression derived here is more general and offers greater insight into the relative effect of the elastic constants. The normalized voltage threshold is shown in Fig. 5(b), where it is clear that the threshold decreases to zero as the actual cell thickness d approaches the critical thickness. The curves also suggest that a lower voltage threshold can be achieved by smaller K_2/K ratios.

3.3 Dynamic Response

To study the dynamic response, we make use of the Ericksen-Leslie dynamic equations [12]. Physically, these represent the three conservation laws (mass, linear momentum and angular momentum). Using the “no-slip” condition, the small angle approximation $\cos\theta \approx 1$ and $\sin\theta \approx \theta$, and the previous assumptions, we arrive at the torque balance equation:

$$\gamma_1 \frac{\partial \theta}{\partial t} = K \frac{\partial^2 \theta}{\partial z^2} + \theta \left(\epsilon_0 \Delta \epsilon E^2 + K \left(\frac{\pi}{d_c} \right)^2 \right) \quad (15)$$

In the above expression $E = V/d$ is the electric field applied and γ_1 is the rotational viscosity. The above equation is solved by

$$\theta(z, t) = \sum_{n=1}^{\infty} A_n \cos\left(\frac{n\pi z}{d}\right) \exp\left(-\frac{t}{\tau_n}\right). \quad (16)$$

By neglecting higher order terms in the above expression, the rise and fall time-constants when $V > V_{th}$ are given by

$$\tau_{on} = \frac{\gamma_1 d^2}{\epsilon_0 \Delta \epsilon (V^2 - V_{th}^2)} \quad \text{and} \quad \tau_{off} = \frac{\gamma_1 d^2}{\epsilon_0 \Delta \epsilon (V_{th}^2)} \quad (17)$$

Note that these exponential rise and fall time constants are related to the 10% to 90% rise (t_{ON}) and fall (t_{OFF}) times through $t_{ON} \sim \ln(9)\tau_{ON}$ and $t_{OFF} \sim \ln(9)\tau_{OFF}$. The ratio of the exponential time constants is shown in Fig. 6(a), and shows the common decrease as the voltage increases. As an initial comparison to experimental data, we plot the predicted switching times for the sample discussed in Ref. [5], using the nematic MLC-6080 (Merck, $\Delta n=0.2$, $K=16.8\text{pN}$, $K_2=7.1\text{pN}$, $\Delta \epsilon=7.2$, $\gamma_1=157\text{mPa}\cdot\text{s}$). While the order of magnitude is similar, we note a major discrepancy between the predicted and experimental switching times (the latter is smaller by factor of ~ 5), which suggests that this two-constant analysis does not capture some of the important dynamic aspects.

4. Conclusion

We analyzed the optical and electrical properties of the LCPG using the FDTD method and the elastic continuum theory. FDTD simulation results show good agreement with analytical expressions for diffractive properties of the periodically aligned LC structure. Furthermore, we anticipate that only a few grating

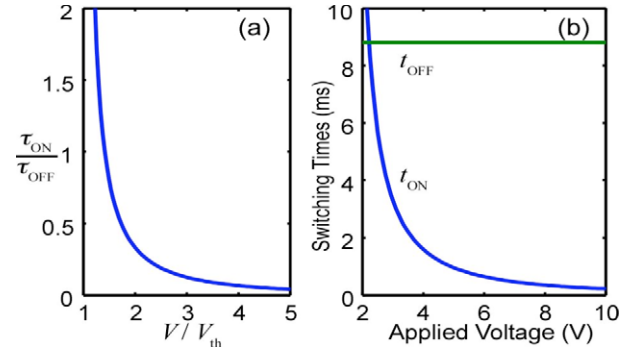


Fig 6: (a) The ratio of the exponential time constants and (b) the estimated dynamic response times (10%-90% measure) for comparison with experimental data [5].

periods are required at a minimum within a pixel to get high diffraction efficiency. The electro-optical performance of the LCPG is based on important parameters like the critical thickness, threshold voltage and the switching times. In this work, we have derived analytical expressions for these parameters under more general assumptions than previously reported.

5. Acknowledgements

The authors gratefully acknowledge the support of the National Science Foundation through a STTR Phase 1 grant (OII 0539552), in partnership with Southeast TechInventures Inc. and ImagineOptix Corp.

6. References

- [1] P. J. Bos, J. Chen, J. W. Doane, B. Smith, C. Holton, and W. Glenn, *J. Info. Display*, vol. **3**, pp. 195-197, 1995.
- [2] J. Chen, P. J. Bos, H. Vithana, and D. L. Johnson, *Appl. Phys. Lett.*, vol. **67**, pp. 2588-2590, 1995.
- [3] C. M. Titus and P. J. Bos, *Appl. Phys. Lett.*, vol. **71**, pp. 2239-2241, 1997.
- [4] Y. Zhang, B. Wang, D. Chung, J. Colegrove, and P.J. Bos, *SID Digest*, vol. **36**, pp. 1178-1181, 2005.
- [5] M.J. Escuti and W.M. Jones, *SID Digest*, vol. **37**, #39.4, 2006.
- [6] L. Nikolov & T. Torodov, *Opt. Acta*, Vol. **31**, 579-588, 1984.
- [7] E. Collett, *Polarized Light*, (M. Dekker: New York, 1993).
- [8] W.M. Jones, B. Conover, and M.J. Escuti, *SID Digest*, Vol. **37**, P-209, 2006.
- [9] J. Schneider and S. Hudson, *IEEE Trans. Antennas and Propagation*, vol. **41**, pp. 994-999, 1993.
- [10] J. A. Roden and S. D. Gedney, *IEEE Trans. Microwave Theory and Techniques*, vol. **46**, pp. 420-427, 1998.
- [11] S. D. Gedney, *IEEE Trans. Antennas and Propagation*, vol. **44**, pp. 1630-1639, 1996.
- [12] I.W. Stewart, *The static and dynamic continuum theory of liquid crystals*, (Taylor & Francis: London, 2004).
- [13] H. Sarkissian, N. Tabirian, B. Park, and B. Zeldovich, *Storming Media Report*, **A000824**, 2004.
- [14] J. N. Eakin, Y. Xie, R. A. Pelcovits, M. D. Radcliffe, and G. P. Crawford, *Appl. Phys. Lett.*, vol. **85**, 1671-1673, 2004.